Mass Determination in SUSY-like Events with Missing Energy

Jack Gunion
U.C. Davis

Collaborators: Hsin-Chia Cheng, Zhenyu Han, Guido Marandella, Bob McElrath

NTHU, 2007

Fundamental physics goals for the LHC and the ILC

1. **Discover and understand in detail the mechanism for EWSB.**

   Higgs bosons, e.g.

2. **Determine if the hierarchy problem has been solved or not.**

   SUSY?

3. **Discover the dark matter particle(s) and measure the properties of all particles needed for computing the relic density.**

   R-parity conserving SUSY for example.

4. **Explain electroweak or other baryogenesis using particles seen at the LHC and ILC.**

Our prejudices are:

- that the LHC will reveal the EWSB mechanism, but that the ILC will be needed to fully detail it;

- that the LHC will also reveal a mechanism that solves the hierarchy/naturalness problems of the SM;

- that if dark matter is a WIMP of any kind, the LHC is very likely to see it, and the ILC should provide the needed detailed measurements in many cases;

- that it is quite possible that LHC + ILC data will provide the info (e.g. Higgs mass, stop masses, .. in SUSY) needed to assess baryogenesis;

Given the probable ILC time scales, the big question is how much will the LHC be able to do on its own, especially as regards items 2) and 3) above.

A very crucial part of the answer involves the accuracy with which mass scales can be determined at the LHC in the presence of missing energy!

Missing Energy: Motivations, Models and Implications

There are two very important reasons to suppose that LHC events will contain missing energy due to a pair of neutral stable weakly-interacting particles.

1. **The correct amount of dark matter relic density is easily achieved if there is a neutral stable TeV scale WIMP — this is almost an independent argument for new physics at the TeV scale.**

   Such a WIMP must be very weakly interacting (if $=$ dark matter) and will therefor 'appear' as missing energy in the LHC detectors.

2. **A new parity associated with the WIMP's (assuming they are at the $\lesssim$ TeV scale) is strongly suggested by precision electroweak data.**

   Precision electroweak observables would be very significantly impacted if there are vertices connecting a single particle of the WIMP family to SM particles.

   If there is a discrete symmetry that only allows a pair of new particles to connect to a SM-particle $\Rightarrow$ all effects at the loop-level.

Then, automatically the lightest particle in this new family will be stable and will escape detection if it is neutral and weakly interacting.

Popular Candidate Models

- **SUSY with R-parity conservation.**

  The lightest supersymmetric particle (LSP) is likely to be a neutralino, which is a good WIMP candidate.

- **Little Higgs Models with T-parity: lightest T-odd particle is a good WIMP.**

- **Universal Extra Dimensions: lightest KK mode (e.g. first excited 'photon') is a good WIMP.**

- **Models with warped unification with Z_3 parity, ...**

All produce events of similar topologies.

The problem: In general, if there is a pair of invisible particles, then there is not enough information to reconstruct the kinematics of each event on an event-by-event basis.

- **Mass scales will be important not only for the dark matter issue but also for the LHC inverse problem: Can we use LHC data to determine the fundamental Lagrangian parameters?**
  And, can we do so with sufficient accuracy as to allow a meaningful extrapolation to the GUT scale?
  The general picture:

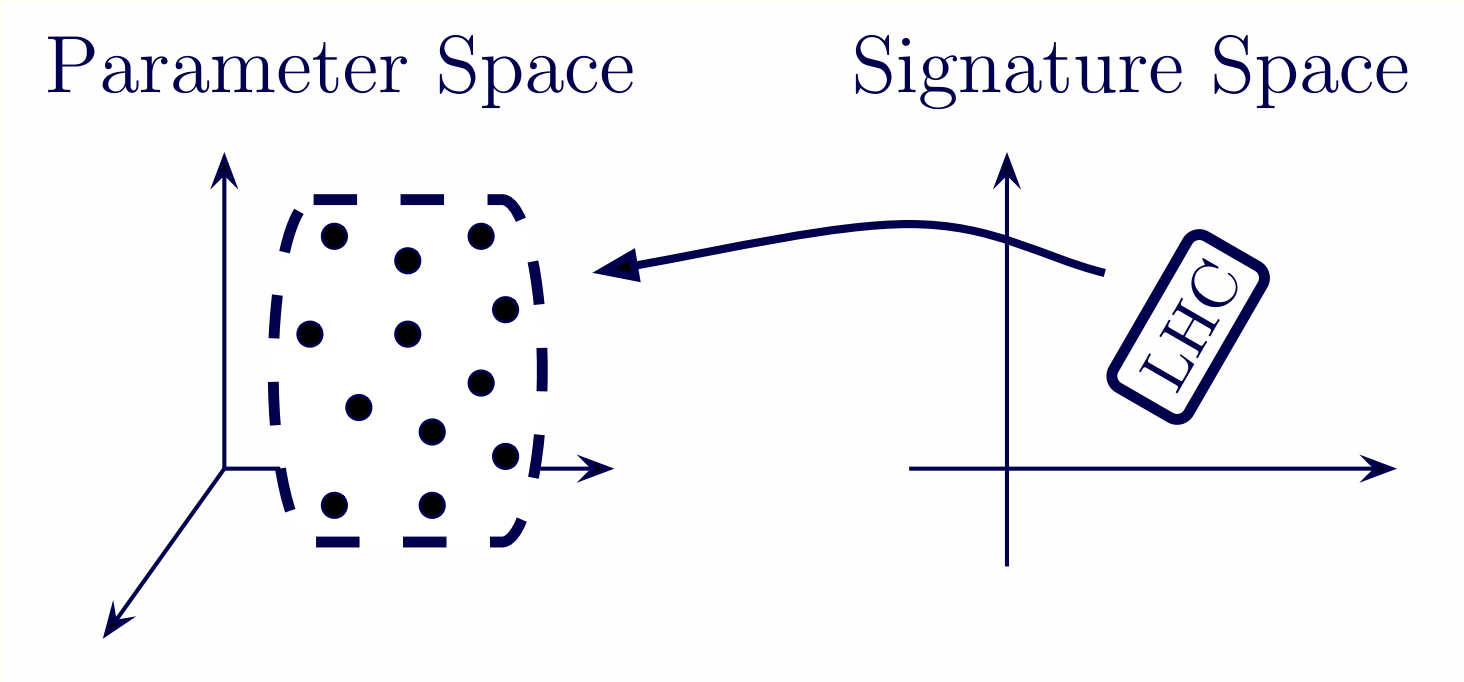

Figure 1: *The likely LHC situation. N. Arkani-Hamed, G. L. Kane, J. Thaler and L. T. Wang, JHEP* **0608**, *070 (2006) [arXiv:hep-ph/0512190].*

This picture presumes that the LHC will have a hard time determining the absolute mass scale. For example, the mSUGRA SPS1a' point gives a

spectrum of the following type:

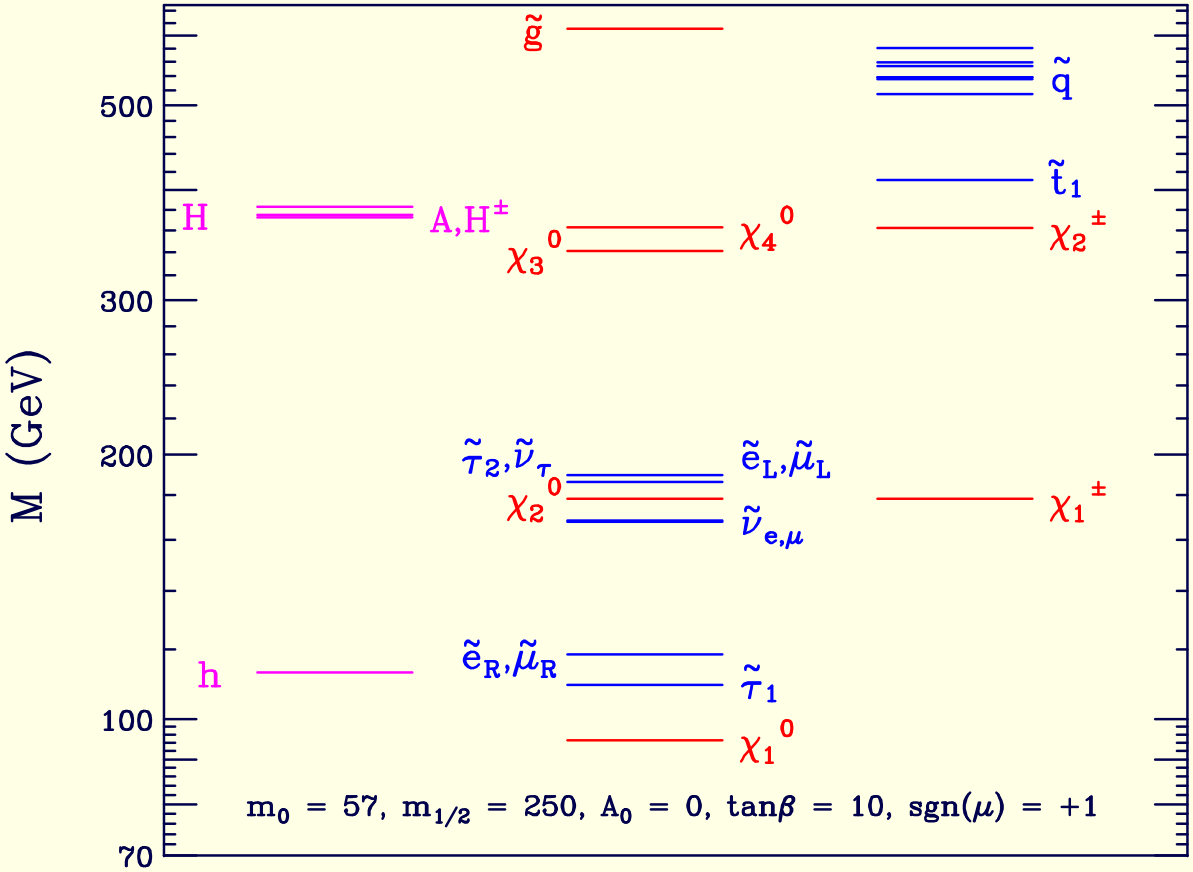

Figure 2: *Mass spectra of an SPS1a'-like point.*

Using lepton spectrum edges and the like, one gets quite a bit of information about the spectrum, but a good determination of the overall mass scale is

elusive. $m_{\tilde{\chi}_1^0}$ sets the overall scale.

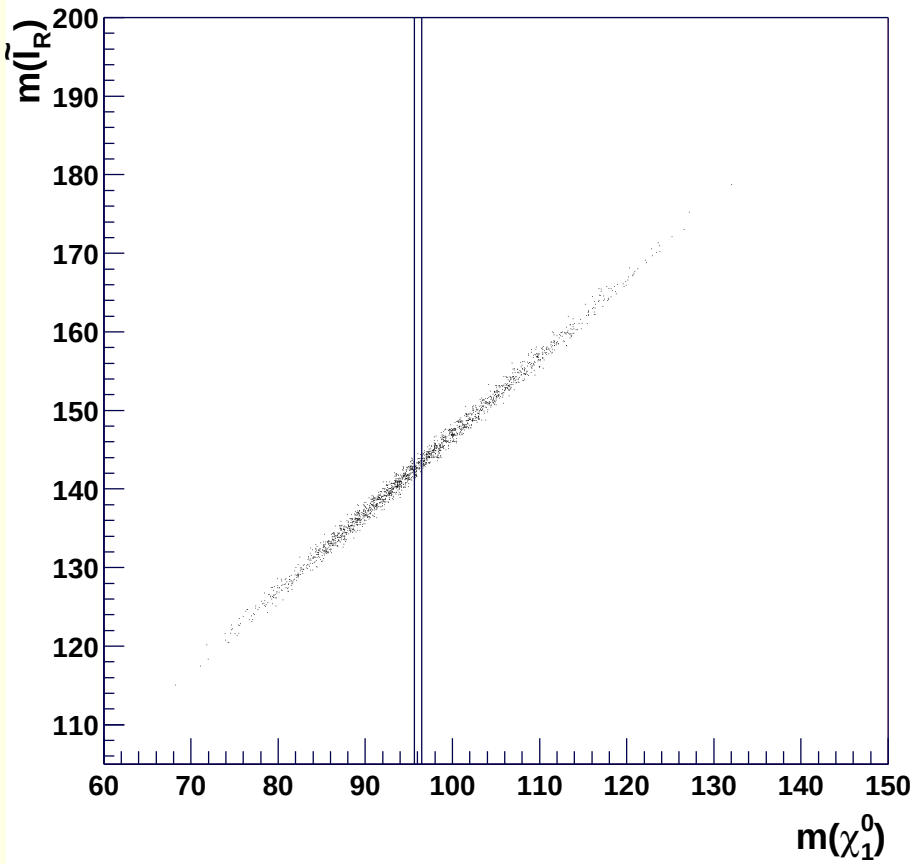

Figure 3: *Sample mass correlation plot. Dots: LHC alone; Vertical band* $= \pm 2\sigma$ *for ILC data. G. Weiglein et al. [LHC/LC Study Group], Phys. Rept.* **426**, *47 (2006) [arXiv:hep-ph/0410364]. Note: These results are for the SPS1a' 'dot'.*

How does the LHC accuracy compare to what is needed?

a) A precision calculation of the dark matter primarily needs accurate masses (couplings being fixed by supersymmetry). The ILC measures $m_{\tilde{\chi}_1^0}$ and other masses to within $\Delta m_{\tilde{\chi}_1^0} \sim \pm 3$ GeV. Could we possibly reach this level at the LHC?

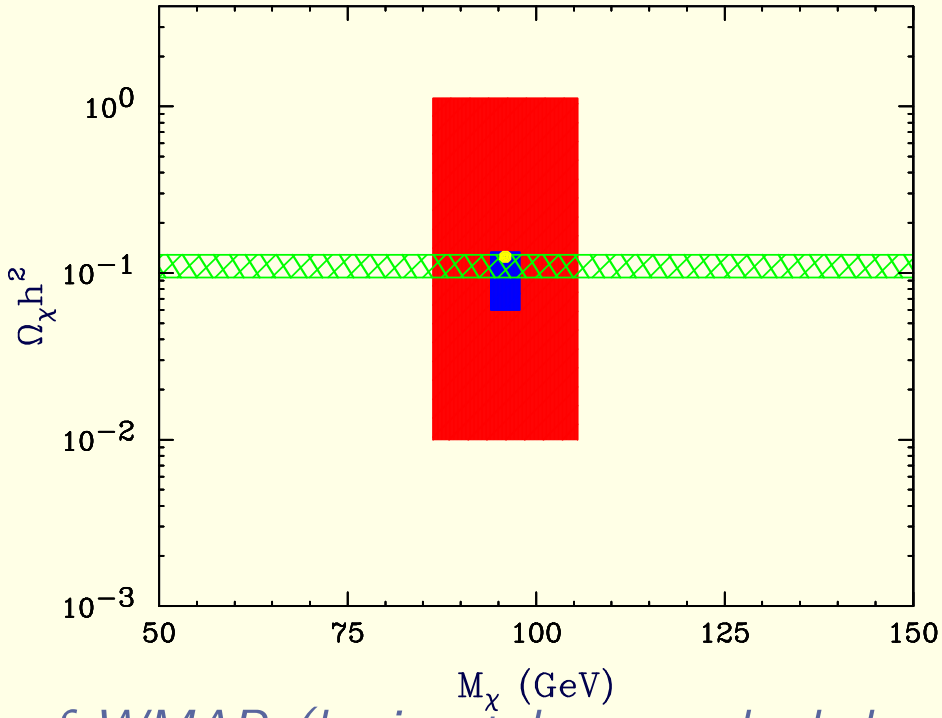

Figure 4: *Accuracy of WMAP (horizontal green shaded region), LHC (outer red rectangle) and ILC (inner blue rectangle) in determining $m_{\tilde{\chi}_1^0}$, the mass of the lightest neutralino, and its relic density $\Omega_\chi h^2$. LHC is assumed to get 10% accuracy on absolute $m_{\tilde{\chi}_1^0}, m_{\tilde{\chi}_2^0}, m_{\tilde{\chi}_1^\pm}$ masses = very optimistic using usual techniques. The yellow dot denotes the actual values of $m_{\tilde{\chi}_1^0}$ and $\Omega_\chi h^2$ for point B'. A. Birkedal, et al.hep-ph/0507214*

b) Precision mass measurement are needed to meaningfully assess GUT scale boundary conditions.

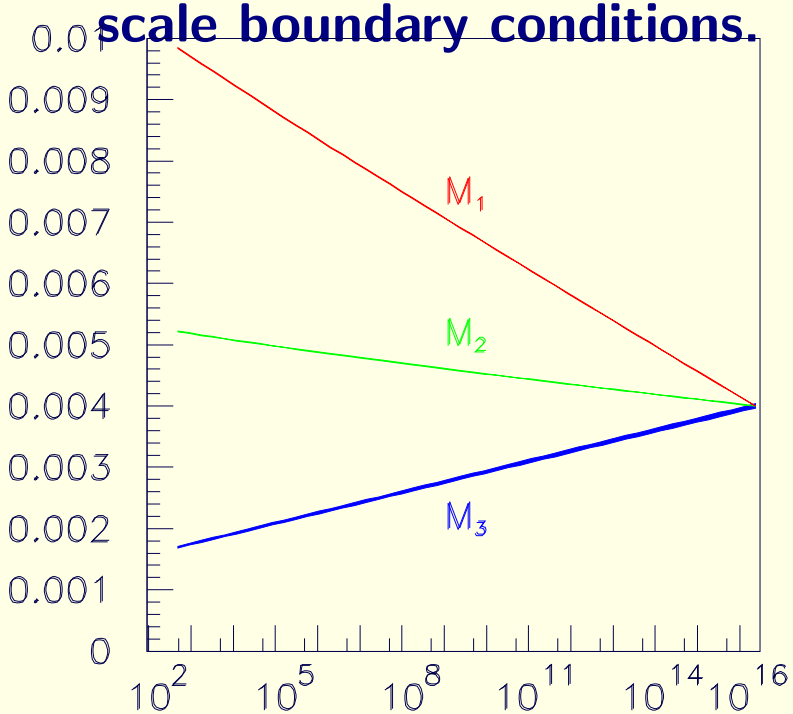

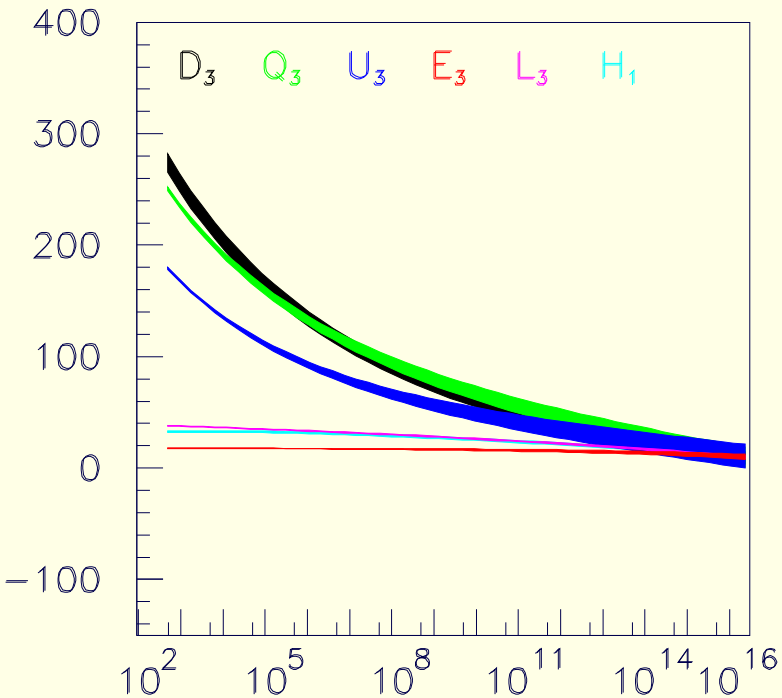

Figure 5: *Evolution to the GUT scale using LHC + ILC1000 measurements. On the left,* $1/M_i$ *[GeV*$^{-1}$*] is plotted vs.* $Q(\text{ GeV})$*. On the right,* $M^2_{\tilde{j}}$ *[*10^3 *GeV*^{2}*] for 3rd soft masses squared are plotted vs.* $Q(\text{ GeV})$*.*

Differences between colored sparticle masses and the weakly interacting sparticle masses are determined at the LHC, and absolute scale for the the latter is possible at the ILC (esp. threshold scans).

We must work to get all (or at least most) of the required accuracy at the LHC.

LHC Review and Developments

- **Observables such as total $\not{E}_T$, H_T, $M_{\rm eff}$ . . . are sensitive to the mass differences of the particles in the decay chains but not very sensitive to the overall mass scale.**

- **If the model is known and all branching ratios for the different chain decay sequences can be computed, then total cross sections for different topologies can be used to determine the absolute scale.**

  But, this is really very model-dependent.

- **One would like to use pure kinematics to get the absolute masses.**

  How well one can do and the best techniques depends very much on the topology of the events.

- **For a long enough chain decay, one can use multiple endpoints. We give a 3-step example below.**

This doesn't work if there are only two visible particles since then there is only one invariant mass that can be formed $\Rightarrow$ too few constraints.

- **For 3-step, look for endpoints in $m_{\ell\ell}$, $m_{q\ell\ell}$, $m_{q\ell}^{high}$, and $m_{q\ell}^{low}$. Gjeltsen, Miller, Osland: hep-ph/0410303**

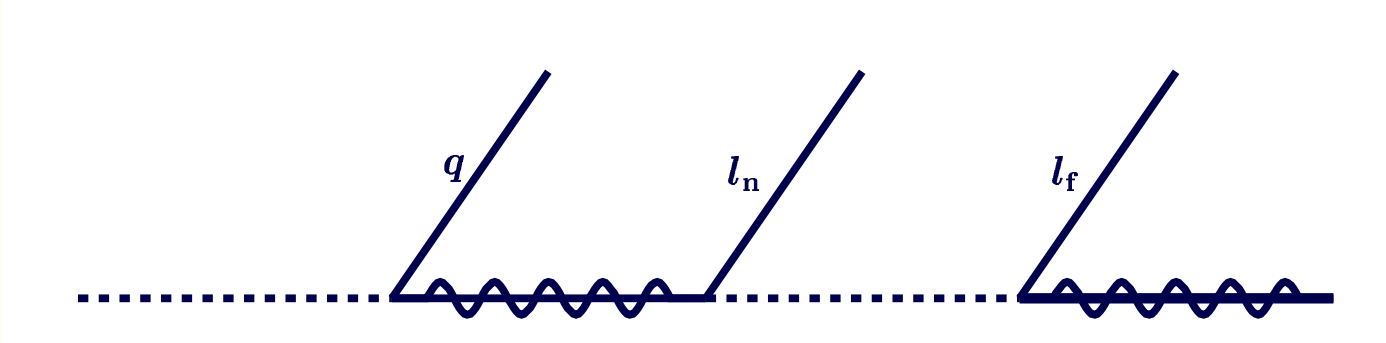

	σ = 32.8 pb	$\tilde{q}_L$	31.4%						1245 fb
(α)	σ = 7.7 pb	$\tilde{b}_1$	35.5%	$\tilde{\chi}_2^0$	12.1%	$\tilde{l}_R$	100%	$\tilde{\chi}_1^0$	329 fb
	σ = 4.3 pb	$\tilde{b}_2$	18.0%						94 fb
									1669 fb
	σ = 3.21 pb	$\tilde{q}_L$	31.9%						54.3 fb
(β)	σ = 0.50 pb	$\tilde{b}_1$	23.6%	$\tilde{\chi}_2^0$	5.3%	$\tilde{l}_R$	100%	$\tilde{\chi}_1^0$	6.3 fb
	σ = 0.31 pb	$\tilde{b}_2$	8.8%						1.5 fb
									62.0 fb

Figure 6: *The SPS1a' type squark decay chain.* $\tilde{q} \to q\ell\ell\tilde{\chi}_1^0$.

$$\left(m_{ll}^{\max}\right)^2 = \left(m_{\tilde{\chi}_2^0}^2 - m_{\tilde{l}_R}^2\right)\left(m_{\tilde{l}_R}^2 - m_{\tilde{\chi}_1^0}^2\right)/m_{\tilde{l}_R}^2$$

$$
\left(m_{qll}^{\max}\right)^2 = \begin{cases}
\dfrac{\left(m_{\tilde{q}_L}^2 - m_{\tilde{\chi}_2^0}^2\right)\left(m_{\tilde{\chi}_2^0}^2 - m_{\tilde{\chi}_1^0}^2\right)}{m_{\tilde{\chi}_2^0}^2} & \text{for} \quad \dfrac{m_{\tilde{q}_L}}{m_{\tilde{\chi}_2^0}} > \dfrac{m_{\tilde{\chi}_2^0}}{m_{\tilde{l}_R}}\dfrac{m_{\tilde{l}_R}}{m_{\tilde{\chi}_1^0}} & (1) \\[2ex]
\dfrac{\left(m_{\tilde{q}_L}^2 m_{\tilde{l}_R}^2 - m_{\tilde{\chi}_2^0}^2 m_{\tilde{\chi}_1^0}^2\right)\left(m_{\tilde{\chi}_2^0}^2 - m_{\tilde{l}_R}^2\right)}{m_{\tilde{\chi}_2^0}^2 m_{\tilde{l}_R}^2} & \text{for} \quad \dfrac{m_{\tilde{\chi}_2^0}}{m_{\tilde{l}_R}} > \dfrac{m_{\tilde{l}_R}}{m_{\tilde{\chi}_1^0}}\dfrac{m_{\tilde{q}_L}}{m_{\tilde{\chi}_2^0}} & (2) \\[2ex]
\dfrac{\left(m_{\tilde{q}_L}^2 - m_{\tilde{l}_R}^2\right)\left(m_{\tilde{l}_R}^2 - m_{\tilde{\chi}_1^0}^2\right)}{m_{\tilde{l}_R}^2} & \text{for} \quad \dfrac{m_{\tilde{l}_R}}{m_{\tilde{\chi}_1^0}} > \dfrac{m_{\tilde{q}_L}}{m_{\tilde{\chi}_2^0}}\dfrac{m_{\tilde{\chi}_2^0}}{m_{\tilde{l}_R}} & (3) \\[2ex]
\left(m_{\tilde{q}_L} - m_{\tilde{\chi}_1^0}\right)^2 & \text{otherwise} & (4)
\end{cases}
$$

$$
\left(m_{ql(\mathrm{low})}^{\max}, m_{ql(\mathrm{high})}^{\max}\right) = \left\{ \begin{array}{llll}
\left(m_{ql_{\mathrm{n}}}^{\max}, m_{ql_{\mathrm{f}}}^{\max}\right) & \text{for} & 2m_{\tilde{l}_R}^2 > m_{\tilde{\chi}_1^0}^2 + m_{\tilde{\chi}_2^0}^2 > 2m_{\tilde{\chi}_1^0} m_{\tilde{\chi}_2^0} & (1) \\
\left(m_{ql(\mathrm{eq})}^{\max}, m_{ql_{\mathrm{f}}}^{\max}\right) & \text{for} & m_{\tilde{\chi}_1^0}^2 + m_{\tilde{\chi}_2^0}^2 > 2m_{\tilde{l}_R}^2 > 2m_{\tilde{\chi}_1^0} m_{\tilde{\chi}_2^0} & (2) \\
\left(m_{ql(\mathrm{eq})}^{\max}, m_{ql_{\mathrm{n}}}^{\max}\right) & \text{for} & m_{\tilde{\chi}_1^0}^2 + m_{\tilde{\chi}_2^0}^2 > 2m_{\tilde{\chi}_1^0} m_{\tilde{\chi}_2^0} > 2m_{\tilde{l}_R}^2 & (3)
\end{array} \right\}
$$

$$
\left(m_{ql_{\mathrm{n}}}^{\max}\right)^2 = \left(m_{\tilde{q}_L}^2 - m_{\tilde{\chi}_2^0}^2\right)\left(m_{\tilde{\chi}_2^0}^2 - m_{\tilde{l}_R}^2\right)/m_{\tilde{\chi}_2^0}^2
$$

$$
\left(m_{ql_{\mathrm{f}}}^{\max}\right)^2 = \left(m_{\tilde{q}_L}^2 - m_{\tilde{\chi}_2^0}^2\right)\left(m_{\tilde{l}_R}^2 - m_{\tilde{\chi}_1^0}^2\right)/m_{\tilde{l}_R}^2
$$

$$\left(m^{\max}_{ql(\mathrm{eq})}\right)^2 = \left(m^2_{\tilde{q}_L} - m^2_{\tilde{\chi}^0_2}\right)\left(m^2_{\tilde{l}_R} - m^2_{\tilde{\chi}^0_1}\right)/\left(2m^2_{\tilde{l}_R} - m^2_{\tilde{\chi}^0_1}\right)$$

$$\begin{aligned}\left(m^{\min}_{qll(\theta>\frac{\pi}{2})}\right)^2 = & \Bigg[\left(m^2_{\tilde{q}_L} + m^2_{\tilde{\chi}^0_2}\right)\left(m^2_{\tilde{\chi}^0_2} - m^2_{\tilde{l}_R}\right)\left(m^2_{\tilde{l}_R} - m^2_{\tilde{\chi}^0_1}\right) \\ & -\left(m^2_{\tilde{q}_L} - m^2_{\tilde{\chi}^0_2}\right)\sqrt{\left(m^2_{\tilde{\chi}^0_2} + m^2_{\tilde{l}_R}\right)^2\left(m^2_{\tilde{l}_R} + m^2_{\tilde{\chi}^0_1}\right)^2 - 16m^2_{\tilde{\chi}^0_2}m^4_{\tilde{l}_R}m^2_{\tilde{\chi}^0_1}} \\ & +2m^2_{\tilde{l}_R}\left(m^2_{\tilde{q}_L} - m^2_{\tilde{\chi}^0_2}\right)\left(m^2_{\tilde{\chi}^0_2} - m^2_{\tilde{\chi}^0_1}\right)\Bigg]/\left(4m^2_{\tilde{l}_R}m^2_{\tilde{\chi}^0_2}\right)\end{aligned}$$

Point	$\tilde{g}$	$\tilde{d}_L$	$\tilde{d}_R$	$\tilde{u}_L$	$\tilde{u}_R$	$\tilde{b}_2$	$\tilde{b}_1$	$\tilde{t}_2$	$\tilde{t}_1$
(α)	595.2	543.0	520.1	537.2	520.5	524.6	491.9	574.6	379.1
(β)	915.5	830.1	799.5	826.3	797.3	800.2	759.4	823.8	610.4
	$\tilde{e}_L$	$\tilde{e}_R$	$\tilde{\tau}_2$	$\tilde{\tau}_1$	$\tilde{\nu}_{e_L}$	$\tilde{\nu}_{\tau_L}$		$H^\pm$	A
(α)	202.1	143.0	206.0	133.4	185.1	185.1		401.8	393.6
(β)	315.6	221.9	317.3	213.4	304.1	304.1		613.9	608.3
	$\tilde{\chi}^0_4$	$\tilde{\chi}^0_3$	$\tilde{\chi}^0_2$	$\tilde{\chi}^0_1$	$\tilde{\chi}^\pm_2$	$\tilde{\chi}^\pm_1$		H	h
(α)	377.8	358.8	176.8	96.1	378.2	176.4		394.2	114.0
(β)	553.3	538.4	299.1	161.0	553.3	299.0		608.9	117.9

Table 1: *Masses [GeV] for the considered SPS 1a points (α: $m_0 = 100$ GeV, $m_{1/2} = 250$ GeV) and (β: $m_0 = 160$ GeV, $m_{1/2} = 400$ GeV).*

For $L = 300\ \mathrm{fb}^{-1}$

	Nom	(1,1) $\langle m \rangle$	(1,1) σ	(1,1) γ_1	(1,2) $\langle m \rangle$	(1,2) σ	(1,2) γ_1
$m_{\tilde{\chi}_1^0}$	96.1	96.3	3.8	0.2	85.3	3.4	0.1
$m_{\tilde{l}_R}$	143.0	143.2	3.8	0.2	130.4	3.7	0.1
$m_{\tilde{\chi}_2^0}$	176.8	177.0	3.7	0.2	165.5	3.4	0.1
$m_{\tilde{q}_L}$	537.2	537.5	6.1	0.1	523.2	5.1	0.1
$m_{\tilde{b}_1}$	491.9	492.4	13.4	0.0	469.6	13.3	0.1
$m_{\tilde{l}_R} - m_{\tilde{\chi}_1^0}$	46.92	46.93	0.28	0.0	45.08	0.72	−0.2
$m_{\tilde{\chi}_2^0} - m_{\tilde{\chi}_1^0}$	80.77	80.77	0.18	0.0	80.18	0.29	−0.1
$m_{\tilde{q}_L} - m_{\tilde{\chi}_1^0}$	441.2	441.3	3.1	0.0	438.0	2.7	0.0
$m_{\tilde{b}_1} - m_{\tilde{\chi}_1^0}$	395.9	396.2	12.0	0.0	384.4	12.0	0.1

Table 2: *SPS 1a (α): Minima for $\Delta\Sigma \leq 1$ in regions (1,1) and (1,2). Ensemble means, $\langle m \rangle$, and root-mean-square distances from the mean, σ, are in GeV. The three lightest masses are very correlated. The mass of $\tilde{q}_L$ is fairly correlated to the lighter masses, but $m_{\tilde{b}_1}$ is essentially uncorrelated. The distributions are very close to symmetric.* **Note the wrong solution region.**

For $L = 300\ \mathrm{fb}^{-1}$

					1 solution			2 solutions					
		(1,1)			(1,2)/(1,3)/B			(1,2)			(1,3)		
	Nom	$\langle m \rangle$	σ	γ_1	$\langle m \rangle$	σ	γ_1	$\langle m \rangle$	σ	γ_1	$\langle m \rangle$	σ	γ_1
$\tilde{\chi}_1^0$	161	438	88	0.9	175	35	1.0	161	22	0.3	166	27	0.6
$\tilde{l}_R$	222	518	85	0.7	236	37	0.8	221	24	0.3	223	28	0.5
$\tilde{\chi}_2^0$	299	579	85	0.7	313	35	1.0	299	22	0.3	304	27	0.6
$\tilde{q}_L$	826	1146	104	0.8	843	44	0.9	826	30	0.3	835	36	0.5
$\tilde{l}_R - \tilde{\chi}_1^0$	61	81	1.8	−0.3	61	4.4	0.4	61	1.9	−0.2	57	1.3	−0.2
$\tilde{\chi}_2^0 - \tilde{\chi}_1^0$	138	141	0.9	0.1	138	0.6	0.2	138	0.5	0.0	138	0.5	0.0
$\tilde{q}_L - \tilde{\chi}_1^0$	665	708	17	0.1	668	10	0.5	665	9	0.1	669	10	0.2

Table 3: *SPS 1a (β): Nominal masses ('Nom') and $\Delta\Sigma \leq 1$ ensemble distribution values for the three solution types. High-mass sector: The (1,1) solutions return masses far beyond the nominal values. Low-mass sector: For the one-solution case the values are based on the common distribution of (1,2), (1,3) and border (B) solutions. In the two-solution case the ensemble variables of both solutions are shown. Ensemble means, $\langle m \rangle$, and root-mean-square values, σ, are in GeV.* **Note how some absolute mass scale solutions are way off.**

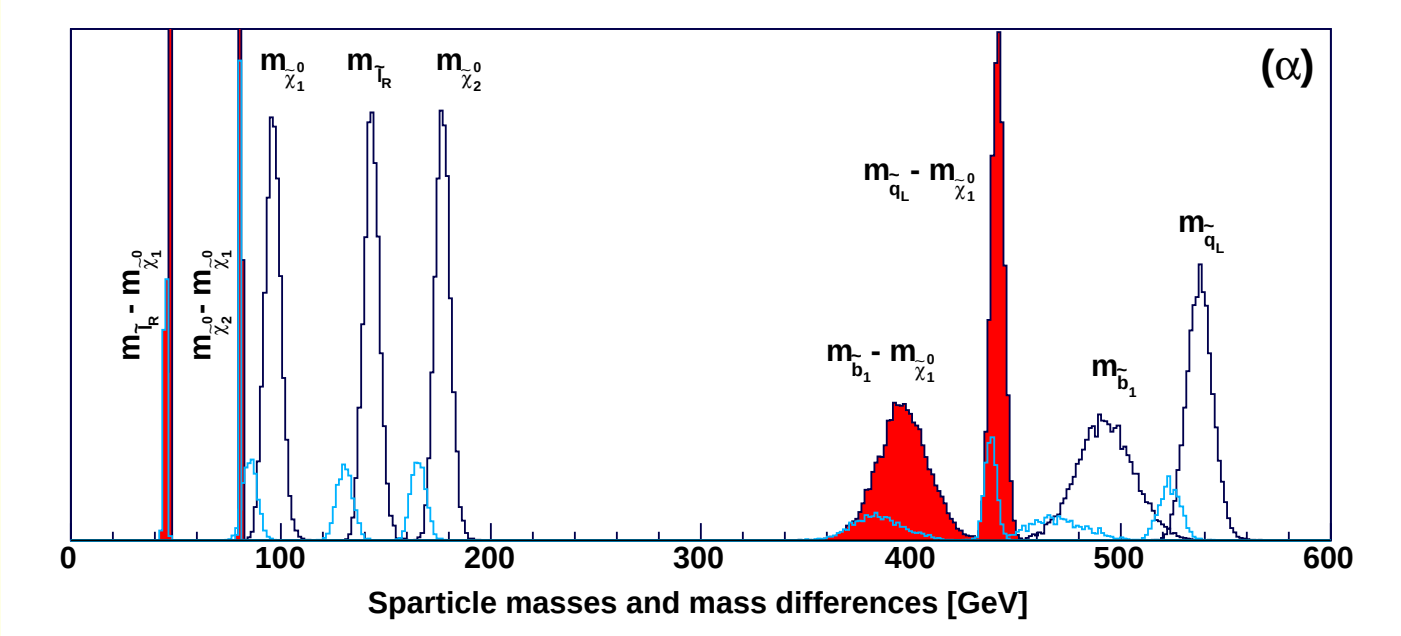

Figure 7: *Plots of mass differences and absolute masses for The SPS1a' type squark decay chain* α.

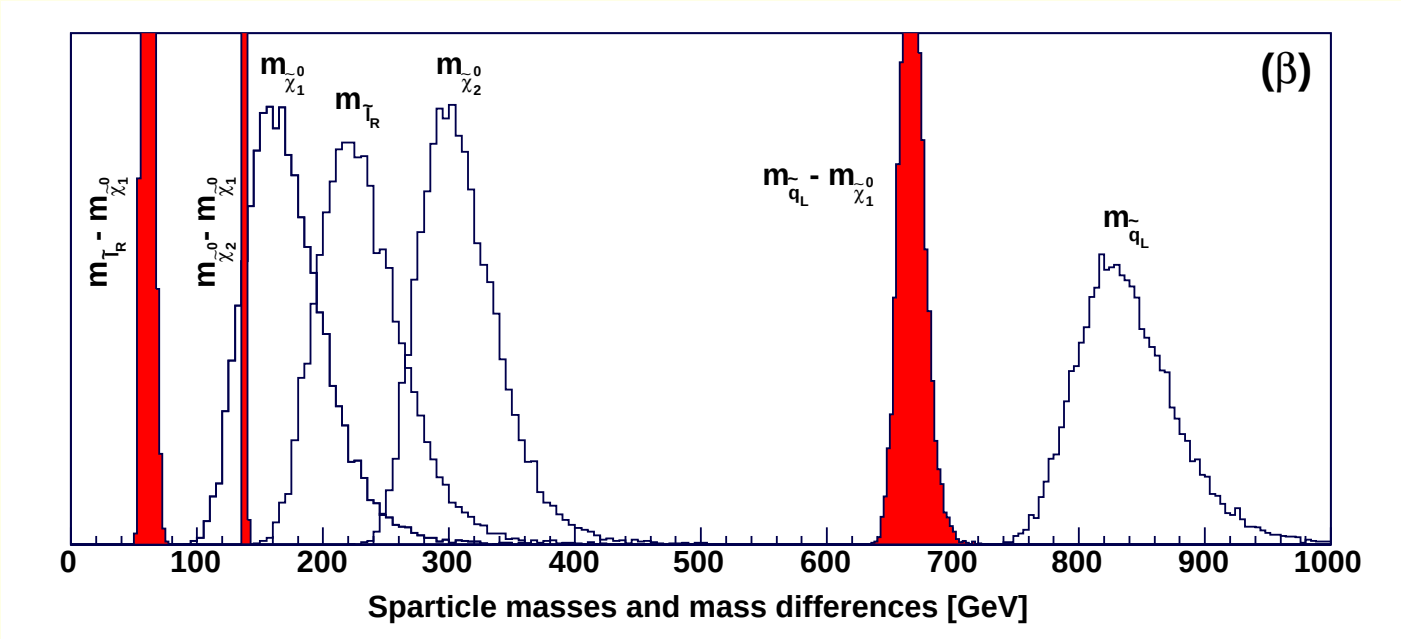

Figure 8: *Plots of mass differences and absolute masses for The SPS1a' type squark decay chain* β.

- **Another analysis of exactly the same decay chain: A.J. Barr, C.G. Lester, M.A. Parker: hep-ph/050843**

  They choose a point consistent with the WMAP data, described by the following set of mSUGRA parameters:

$$m_0 = 70 \text{ GeV},\ m_{1/2} = 350 \text{ GeV},\ \tan\beta = 10,\ A_0 = 0,\ \mu > 0$$

yielding

Particle	Mass (GeV)
$\tilde{\chi}_1^0$	137
$\tilde{\chi}_2^0$	264
$\tilde{e}_L$	255
$\tilde{e}_R$	154
$\tilde{g}$	832
$\tilde{u}_L$	760
$\tilde{u}_R$	735
$\tilde{d}_L$	764
$\tilde{d}_R$	733

Particle	Mass (GeV)
$\tilde{b}_1$	698
$\tilde{b}_2$	723
$\tilde{t}_1$	574
$\tilde{t}_2$	749
$\tilde{\tau}_1$	147
$\tilde{\tau}_2$	257
h	116

Table 4: *The most important sparticle masses at the coannihilation point.*

$$L = 100 \text{ fb}^{-1}$$

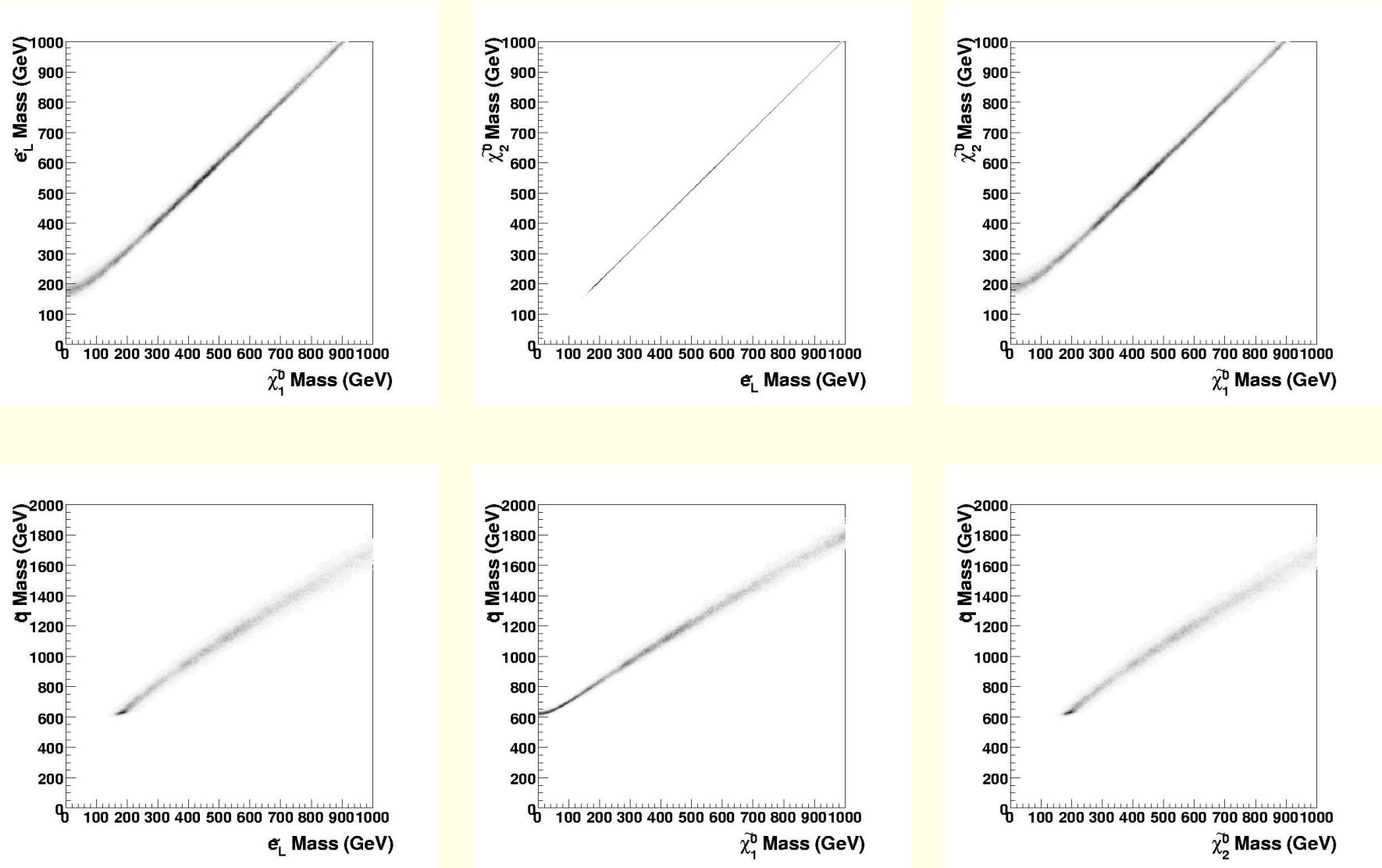

Figure 9: *The region of mass space consistent with the kinematic edge measurements described in the text, obtained using a Markov chain sampler.*

$L = 100\ \mathrm{fb}^{-1}$

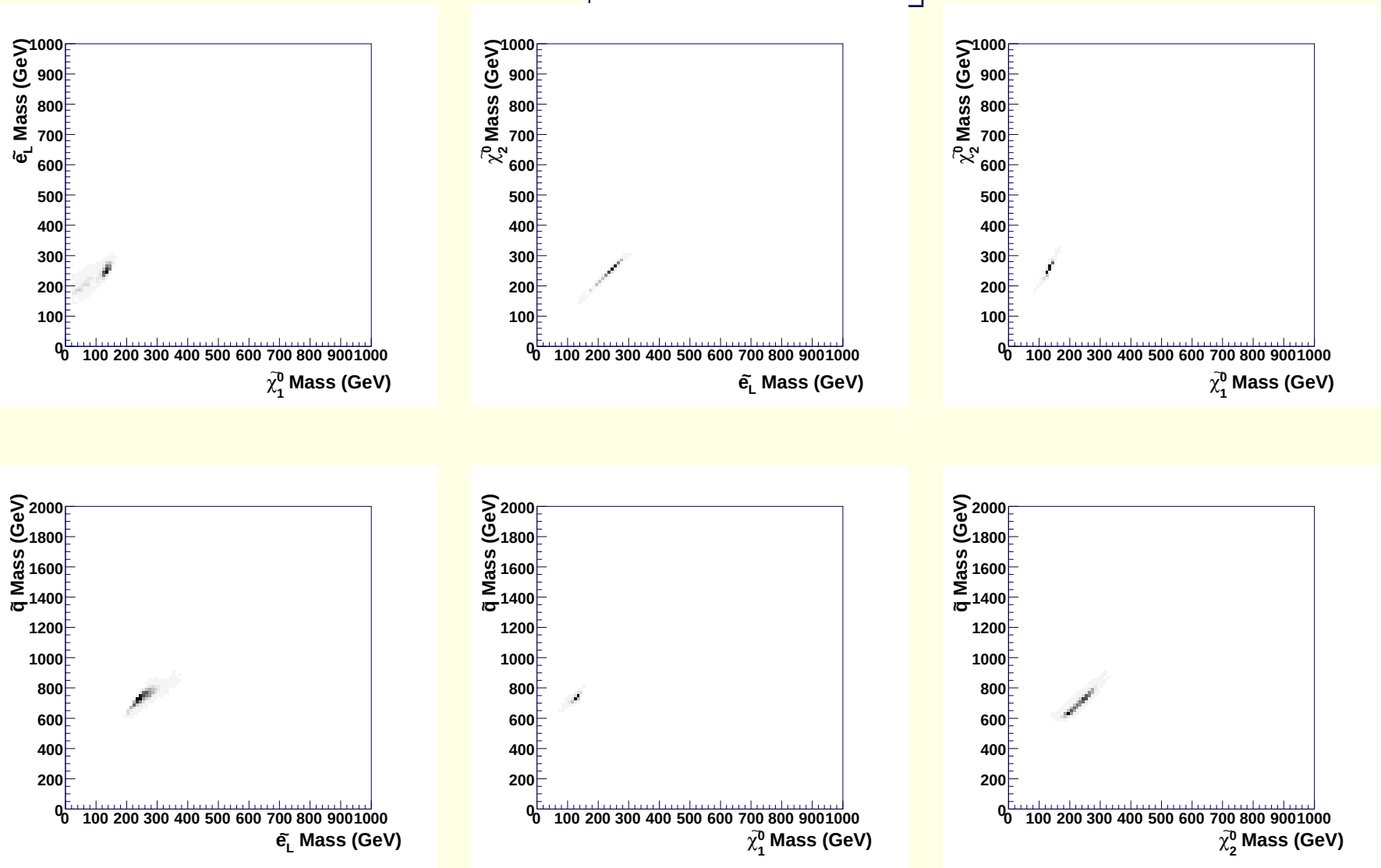

Figure 10: *The region of mass space consistent with a measurement at 10% precision of the cross-section of events with missing p_T greater than 500 GeV, overlapped with a measurement of the squark decay kinematic endpoints. Much better, but model-dependent and still not wonderful.*

- **An approach that comes closer to ours is that of Kawagoe, Nojiri, Polesello, hep-ph/0312317, hep-ph/0410160.**

  They consider a very long decay chain:

$$\widetilde{g} \to \widetilde{b} b_2 \to \widetilde{\chi}_2^0 b_1 b_2 \to \widetilde{l} b_1 b_2 \ell_1 \to \widetilde{\chi}_1^0 b_1 b_2 \ell_1 \ell_2 \tag{8}$$

  The constraint equations are:

$$\begin{aligned} m^2_{\widetilde{\chi}_1^0} &= p^2_{\widetilde{\chi}_1^0} \\ m^2_{\widetilde{\ell}} &= (p_{\widetilde{\chi}_1^0} + p_{\ell_1})^2 \\ m^2_{\widetilde{\chi}_2^0} &= (p_{\widetilde{\chi}_1^0} + p_{\ell_1} + p_{\ell_2})^2 \\ m^2_{\widetilde{b}} &= (p_{\widetilde{\chi}_1^0} + p_{\ell_1} + p_{\ell_2} + p_{b_1})^2 \\ m^2_{\widetilde{g}} &= (p_{\widetilde{\chi}_1^0} + p_{\ell_1} + p_{\ell_2} + p_{b_1} + p_{b_2})^2 \end{aligned} \tag{9}$$

  For each event there are 4 unknowns (the components of $p_{\widetilde{\chi}_1^0}$). However, every event is presumed to have the same set of five masses.

  Thus, after n events we have $5 + 4n$ unknowns (the 5 coming from the five unknown masses) and $5n$ constraints (again the 5 is the assumed 5 masses).

To solve, we must have #unknowns=#constraints:

$$5 + 4n = 5n \,, \Rightarrow n = 5 \,. \tag{10}$$

In other words, after just $n = 5$ events we can solve.

Indeed, for each set of 5 events, we should get a unique solution in principle, and all should agree.

In practice, this is not what they did.

Before going on, the important point of the long chain decay should now be clear.

Even though there are two neutralinos produced in each collider event, *if we can isolate the* $\mathbf{3}$ *visible particles in the decay of a given gluino* **then we don't care about what the other gluino is doing. It will just add to our statistics.**

Well, there are combinatorics/misassignment issues here of course.

Anyway, what they actually did in their papers is as follows.

They assume that $m_{\tilde{\chi}_1^0}$, $m_{\tilde{\chi}_2^0}$ and $m_{\tilde{\ell}}$ are measured from endpoints (maybe also ILC) with great precision (as we have seen, if we only have LHC data this is not so perfect an assumption).

In this case, the unknown masses are $m_{\tilde{g}}$ and $m_{\tilde{b}}$.

For n events we have $2 + 4n$ unknowns and $5n$ constraints (keeping in mind that we assume or know masses for all five particles). $2 + 4n = 5n$ implies that in a perfect world we only need $n = 2$ events to get a unique solution.

In reality, there are backgrounds and the final result is phrased in terms of likelihood contours. The current problem in their words is:

"The likelihood distribution peaks at the gluino and sbottom mass difference as 99.5 GeV for $\tan\beta = 10$, 104.2 GeV for $\tan\beta = 15$, and 113.9 GeV for $\tan\beta = 20$, where the input value is 103.3 GeV, 109.9 GeV and 116.5 GeV, respectively. The fitted values display shift of about 4 GeV from the true value. We ascribe this effect to our simplified modeling of the jet smearing in building the likelihood function, which should disappear once the detector response is properly taken into account in the unfolding procedure."

Well, there is a lot hidden in this phrase, but a very thorough understanding of the detector is clearly required.

- With this long-winded warm-up, I now turn to our procedure which we claim is: a) more robust; b) of greater general applicability; c) yields at the moment similar errors, but with further improvement likely.

Our Approach

- **We claim that one can do well at the LHC by taking a more global point of view and using as much information as is available in every event.**

  Our approach can be applied to many different types of event topologies, but here we focus on a subcomponent of the SPS1a type event in a way that has not been previously attempted.

  Consider the chain decay sequence:

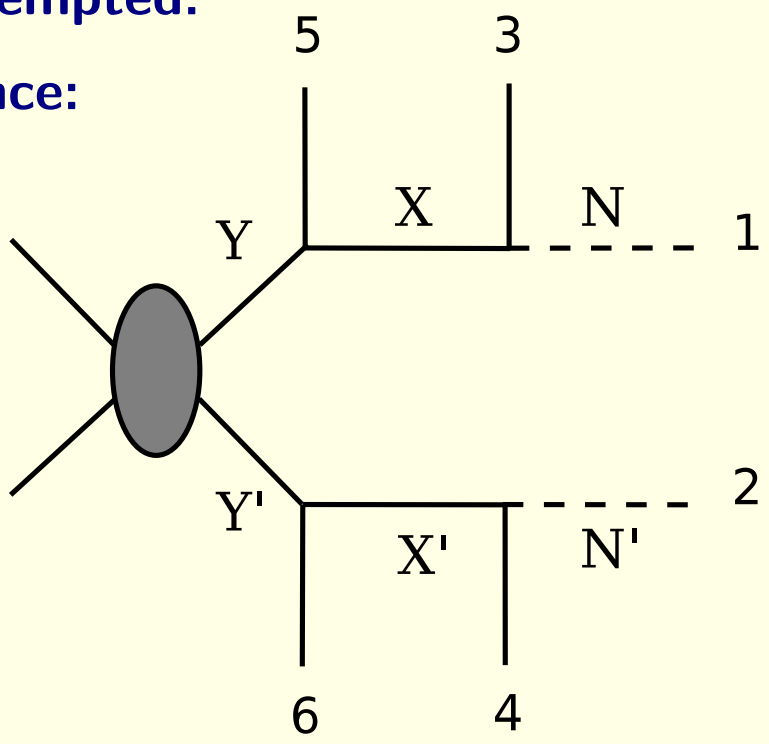

Figure 11: *A typical chain decay topology.*

Note: some cuts to isolate a given topology are required (just as in the previous analyzes) — perhaps OSET would do the job. By this, we don't mean perfect isolation — roughly a ratio of $S/B > 2$ is certain to work, where B could include old physics and new physics signals of other topologies. Even $S/B \sim 1$ is probably workable.

This topology can be applied to many processes with 4 visible and 2 invisible particles.

For example, suppose $M_Y = M_{Y'}$, $M_X = M_{X'}$, and $M_N = M_{N'}$.

Examples that fit this:

$$
\begin{aligned}
t\bar{t} &\to bW^+bW^- \to bl^+\nu bl^-\bar{\nu} \\
\tilde{\chi}_2^0\tilde{\chi}_2^0 &\to l\tilde{l}l\tilde{l} \to ll\tilde{\chi}_1^0 ll\tilde{\chi}_1^0 \\
\tilde{q}\tilde{q} &\to q\tilde{\chi}_2^0 q\tilde{\chi}_2^0 \to ql\tilde{l}ql\tilde{l} \to qll\tilde{\chi}_1^0 qll\tilde{\chi}_1^0 \\
\tilde{t}\bar{\tilde{t}} &\to b\tilde{\chi}^+\bar{b}\tilde{\chi}^- \to bW^+\tilde{\chi}_1^0\bar{b}W^-\tilde{\chi}_1^0
\end{aligned}
$$

The third entry above is the SPS1a' case of interest.

Let us count the constraints and unknowns. For this we (temporarily) assume that the particles are exactly on-shell and that experimental resolutions are perfect.

1. There are 8 unknowns corresponding to the 4-momenta of the N and N'.

2. There are 2 constraints on these coming from knowledge of the visible transverse momenta. (We are assuming that the longitudinal momentum and energy of the collision is not known, as appropriate at a hadron collider.)

   If there are extra visible jets in the event we just include them in visible p_T.

   The visible particles 3, 4, 5 and 6 need not be stable. We just need to be able to determine their 4-momenta (e.g. $W \to jj$ is ok but $W \to \ell\nu$ is not).

3. There are the 3 constraints coming from requiring the equalities: $M_Y = M_{Y'}$, $M_X = M_{X'}$, and $M_N = M_{N'}$.

4. If we know the 3 masses, then we can solve for the 4-momenta of the N and N' and vice versa.

The equations are quartic, and so there can be 4, 2 or 0 solutions (with acceptable positive real energies for the N and N').

5. For each event, we scan through the mass space to see if one or more of the discrete solutions is acceptable.

   Each event then defines a 3-dimensional region in the 3-dimensional mass space that is physically acceptable.

6. As we increase the number of events the 3-dimensional mass region consistent with all events becomes smaller.

   However, in general (and in practice) this region will not shrink to a point.

   Thus, we need additional methods to pick out the correct point in mass space.

- To illustrate our approach, we can consider the explicit example

$$\begin{gathered} \widetilde{\chi}_2^0 \widetilde{\chi}_2^0 \to \ell\widetilde{\ell}\ell\widetilde{\ell} \to \ell\ell\widetilde{\chi}_1^0\ell\ell\widetilde{\chi}_1^0 \\ i.e. \quad Y = Y' = \widetilde{\chi}_2^0, \quad X = X' = \widetilde{\ell}, \quad N = N' = \widetilde{\chi}_1^0 \,, \end{gathered} \quad ,$$

which we generate as a subcomponent of

$$\widetilde{q}\widetilde{q} \to q\widetilde{\chi}_2^0 q\widetilde{\chi}_2^0 \to \ldots \to q\ell\ell\widetilde{\chi}_1^0 q\ell\ell\widetilde{\chi}_1^0 \,. \tag{11}$$

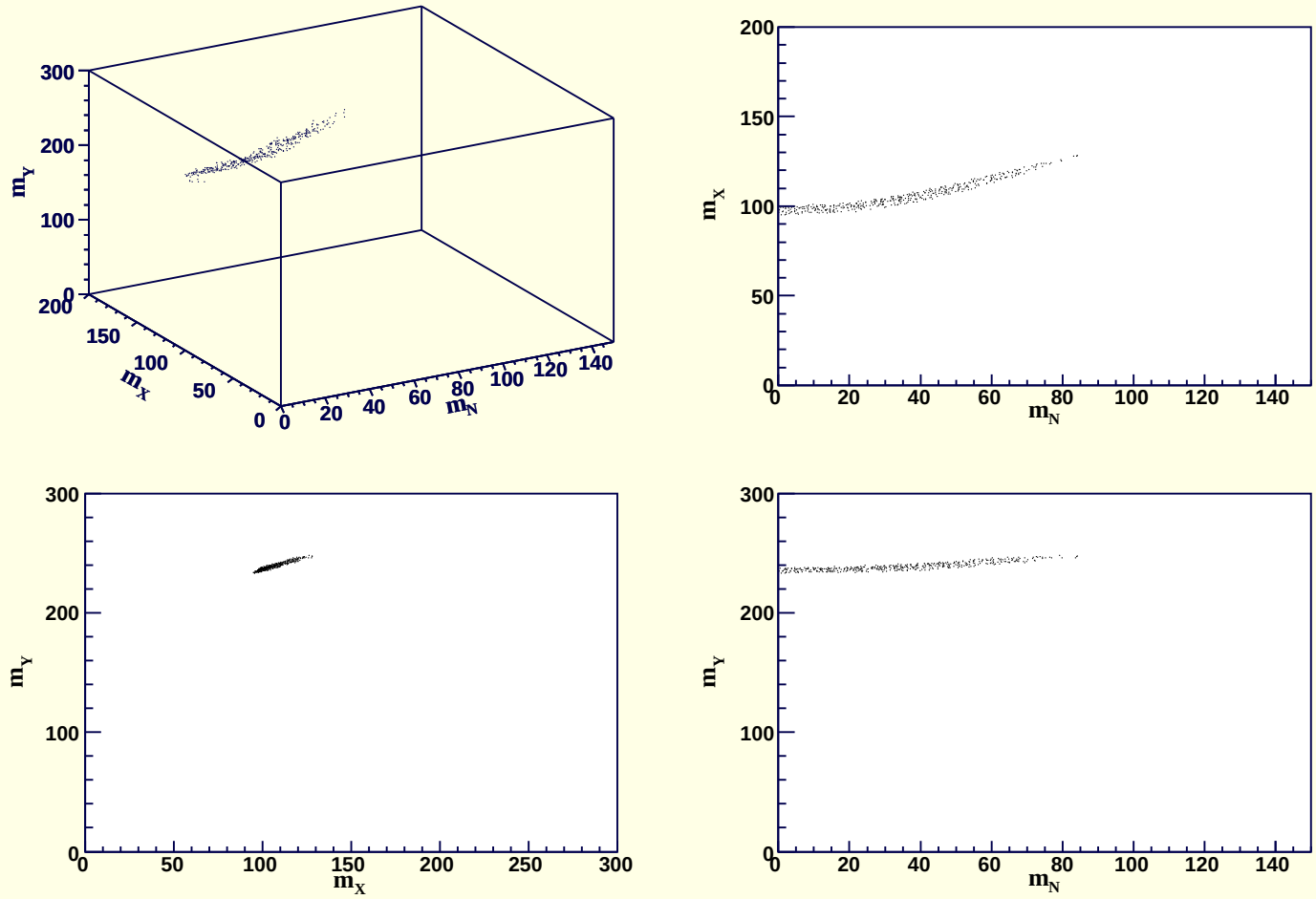

Figure 12: *Mass region (in GeV) that can solve all events.* $\mathbf{500}$ *generated events for* $m_Y = \mathbf{246.6}$ GeV, $m_X = \mathbf{128.4}$ GeV *and* $m_N = \mathbf{85.3}$ GeV, *using correct chain assignments and perfect resolution.*

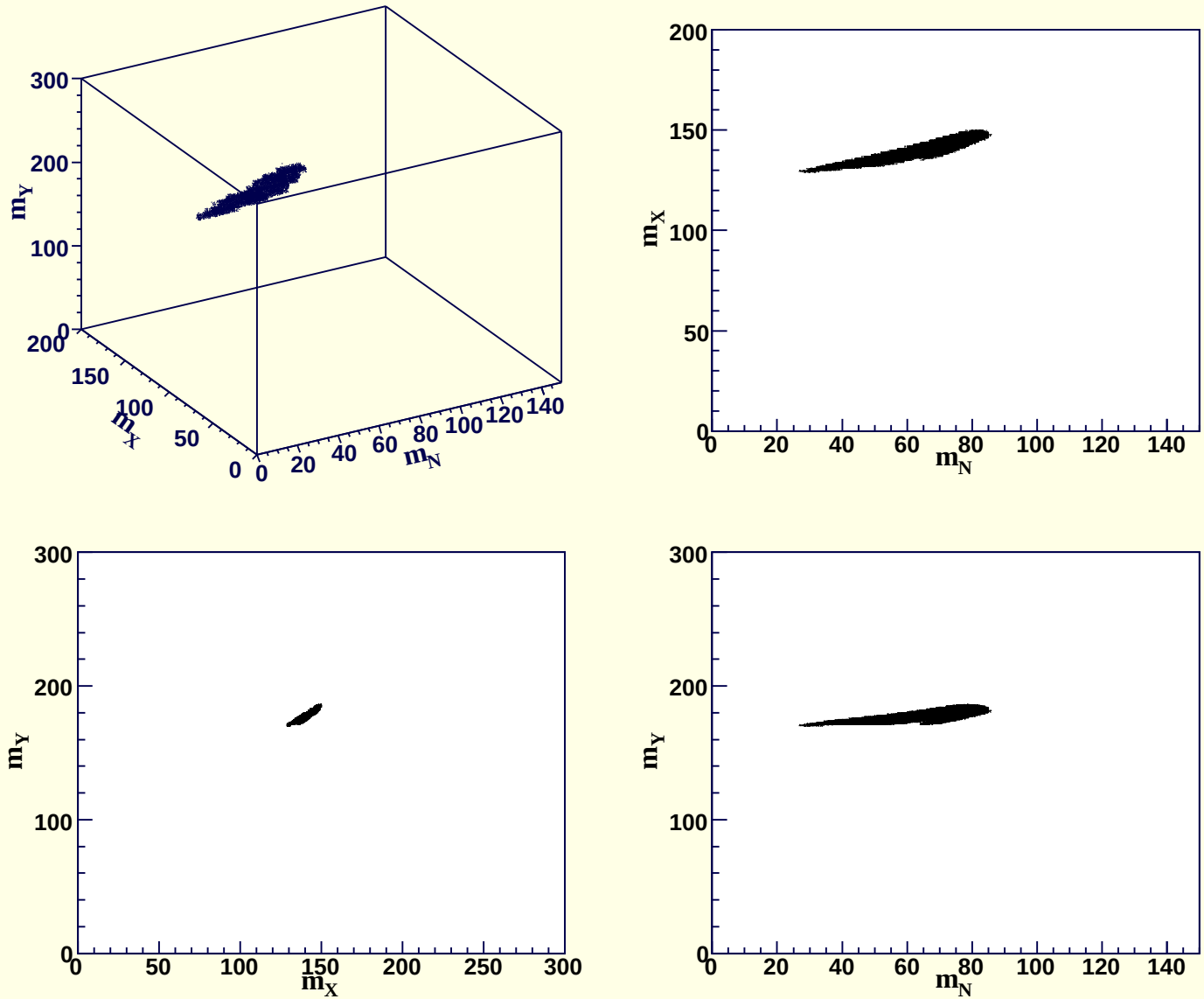

Figure 13: *Mass region (in GeV) that can solve all events.* $\mathbf{500}$ *generated events for* $m_Y = \mathbf{180.8}$ GeV, $m_X = \mathbf{147.1}$ GeV *and* $m_N = \mathbf{85.2}$ GeV, *using correct chain assignments and perfect resolution.*

We found that the correct masses lie at the end point of the allowed region. A graphical picture is:

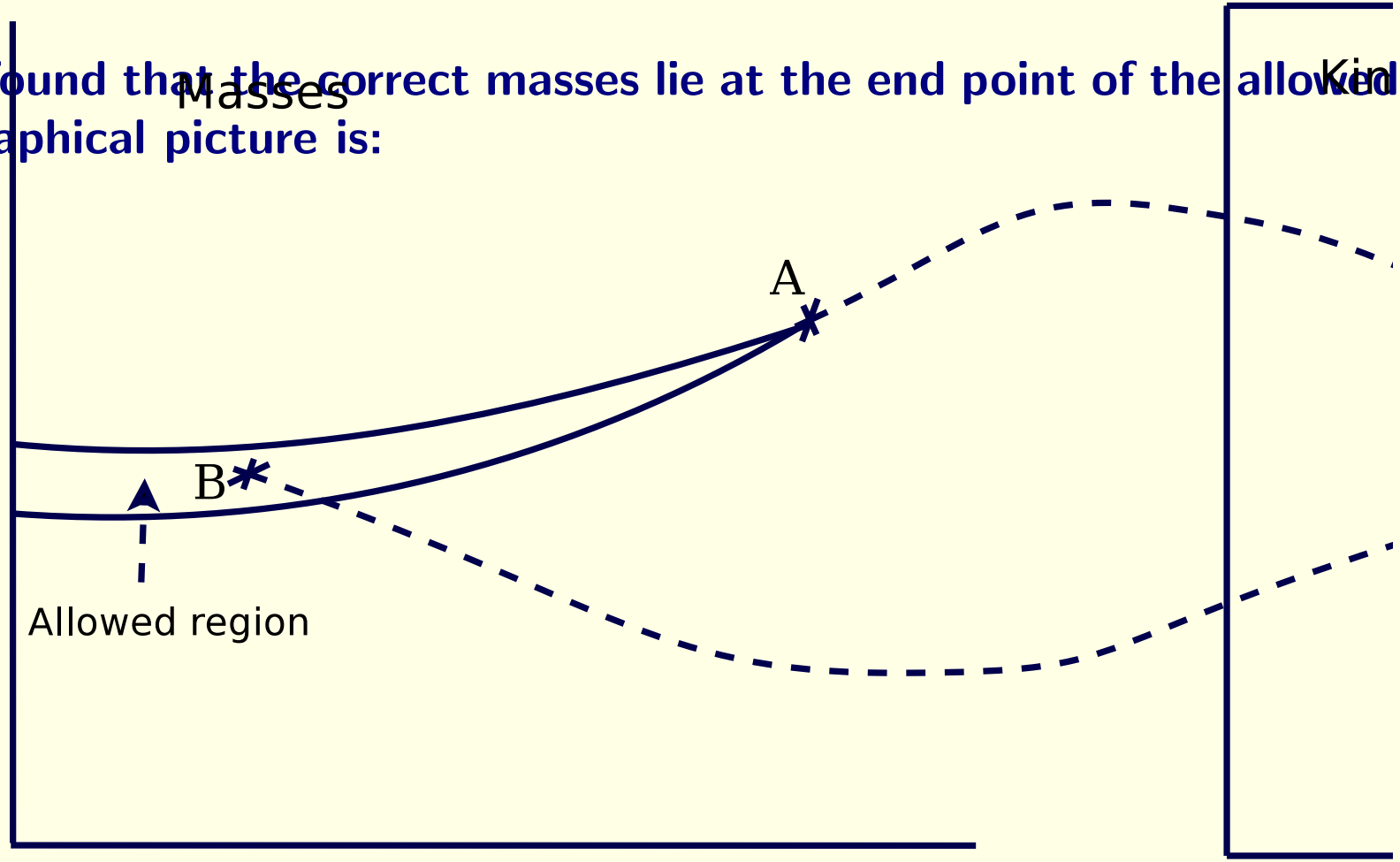

Figure 14: *Map between mass space and kinematic space. The nominal masses, point A, produces a kinematic region that coincides with the experimental region: $\mathcal{K}_A = \mathcal{K}_{exp}$. A point B inside the allowed mass region produces a larger kinematic region: $\mathcal{K}_B \supset \mathcal{K}_{exp}$.*

a) The correct set of masses, $\mathcal{M}$ at point A in Fig. 14, produces a kinematic

region $\mathcal{K}_A$ that coincides with the experimental one, $\mathcal{K}_A = \mathcal{K}_{exp}$, as long as the experimental statistics is large enough.

b) A different mass point produces a region that is either smaller or larger than $\mathcal{K}_{exp}$[1].

c) If smaller, the mass point does not appear in the mass region allowed by all events.

d) If larger, it does, and we denote this kind of point, with mass set $\mathcal{M}'$, as point B in Fig. 14.

e) Let us shift the masses slightly to $\mathcal{M}' + \delta\mathcal{M}'$.

- If the resulting kinematic region still covers $\mathcal{K}_{exp}$, then $\mathcal{M}' + \delta\mathcal{M}'$ is still within the allowed region.
- Apparently, point B, which produces a region larger than K_{exp}, has the freedom to move in all directions and must live inside the allowed region.
- On the other hand, the correct mass point A, which produces exactly $\mathcal{K}_{exp}$, has the least freedom to move and must be located at an end point of the allowed region.

However, With finite masses and resolutions, not all events can be solved by the correct mass point.

[1] In general cases, there could exist degenerate points that produce exactly the same kinematic region as the correct one. It is impossible to raise the degeneracy using pure kinematics.

$\Rightarrow$ **the correct mass point will not lie within the intersection region (assuming there is any such region left).**

We also need to include combinatorics as we don't know which leptons go with which chain decay.

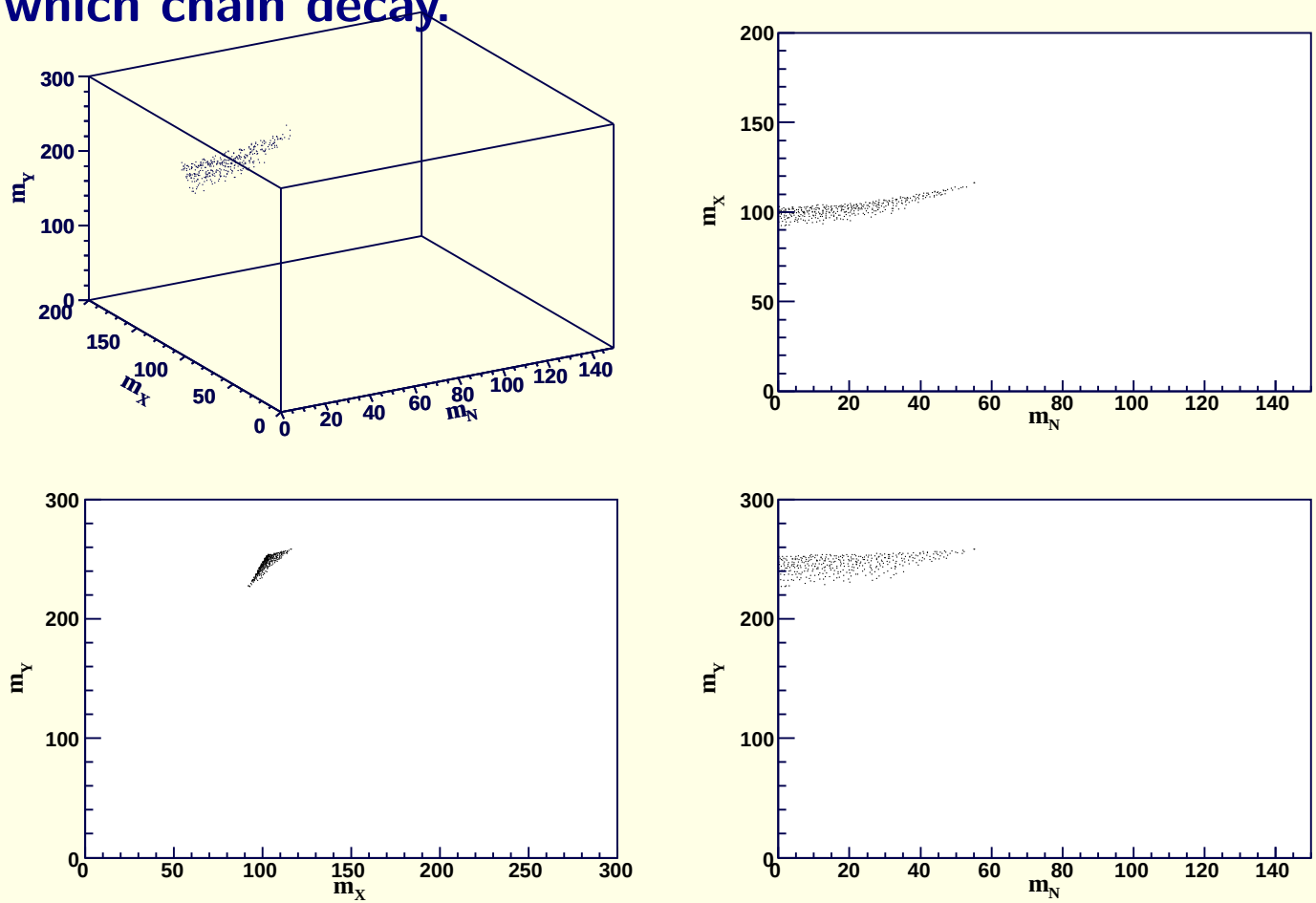

Figure 15: *The allowed mass region (in* GeV*) with smearing (ALTFAST) and wrong combinatorics.* $\mathbf{500}$ *generated events for* $m_Y = \mathbf{246.6}\ \mathrm{GeV}, m_X = \mathbf{128.4}\ \mathrm{GeV}$ *and* $m_N = \mathbf{85.3}\ \mathrm{GeV}$*. Cuts:* $|\eta| < \mathbf{2.5}$*,* $p_T(\ell) > \mathbf{6}\ \mathrm{GeV}$*.*

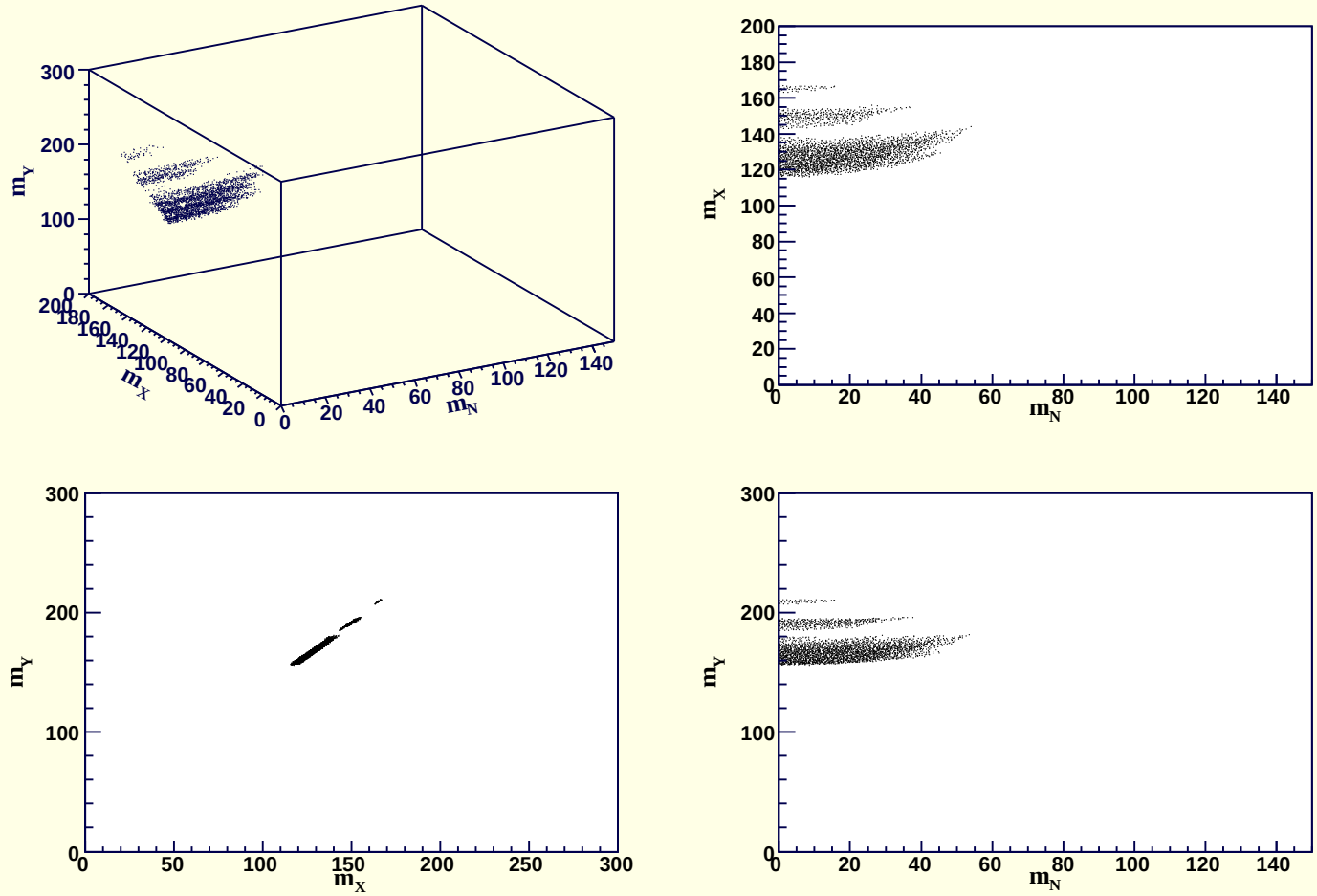

Figure 16: *Mass region (in* GeV*) that can solve all events.* $\mathbf{500}$ *generated events for* $m_Y = 180.8\ \mathrm{GeV}, m_X = 147.1\ \mathrm{GeV}$ *and* $m_N = 85.2\ \mathrm{GeV}$*, after smearing, combinatorics and cuts.*

- **In the more realistic case, the correct mass choices do not correspond to an endpoint but rather correspond to the choices such that changes in the masses result in the most rapid decline in the number of solved/consistent events.**

- **Looking for this point of steepest decline in a 3-dimensional space is numerically difficult.**

- **If we fix two of the masses, and vary the $3rd$ mass, then we can usually identify the point at which the number of solved events starts a steep decline as this $3rd$ mass is changed.**

  This will allow an iterative approach.

- **The approach that works is to cycle through the $3rd$-mass choices, and at each stage look for the peak in the number of solved/consistent events as a function of this $3rd$-mass.**

  The 'peaks' are actually obtained by the intersection of the two fitted straight lines illustrated in the following figure, where two masses are set to their correct values and the $3rd$-mass is varied.

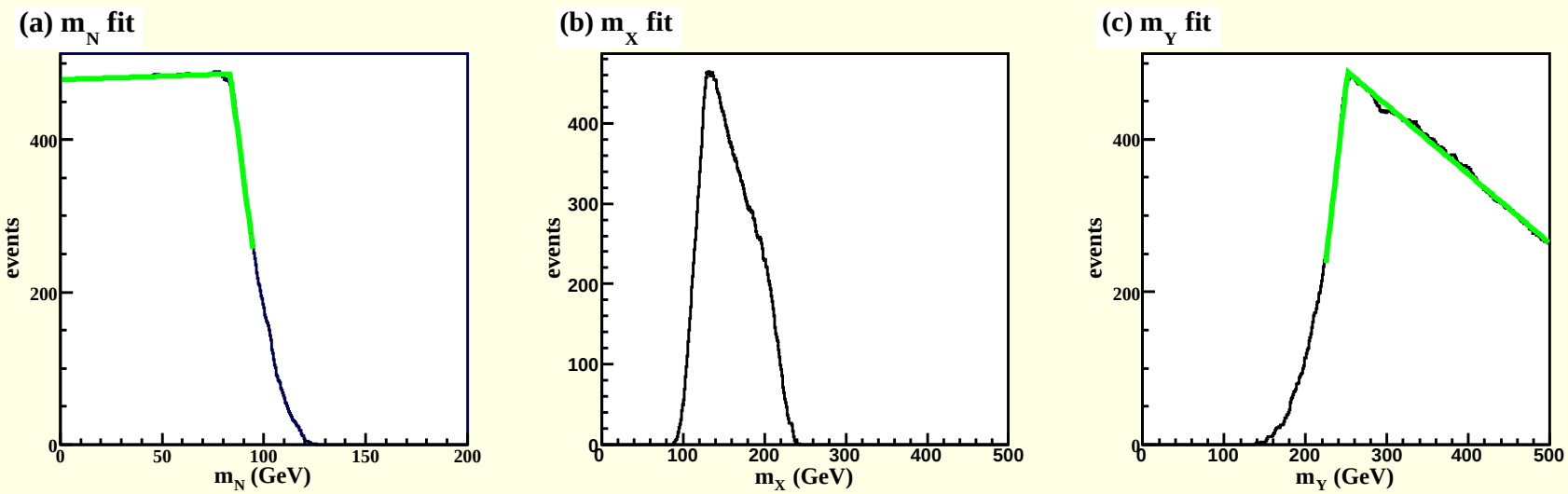

Figure 17: *One-dimensional fits by fixing the other two masses at the correct values. 500 events, combinatorics, smearing and simple cuts included. Peaks are close to correct masses.*

- **We now get more realistic still.**

  Generate 50 fb^{-1} at the LHC, with the same masses as above.

  Take into consideration the decay branching ratios, $\Rightarrow$ roughly 2900 events.

  Initial and final state radiation, experimental resolutions and combinatorics (assuming $\ell = \mu$ for all, which is the worst case) are all included .

To reduce the SM background, we require that all muons are isolated and pass the kinematic cuts:

$$|\eta|_\mu < 2.5, \quad P_{T\mu} > 10 \text{ GeV}, \quad \not{p}_T > 50 \text{ GeV}. \tag{12}$$

With these cuts, the four-muon SM background is negligible.

The number of signal events is reduced from 2900 to about 1900.

The procedure to get the masses comprises the following steps:

1. Randomly select a set of masses $m_Y > m_X > m_N$ that is below the correct masses (for example, the current experimental limits).
2. Do one dimensional recursive fits in the order of m_Y, m_X, m_N with the other two masses fixed. A few intermediate one-dimensional fits are

shown in Fig. 18.

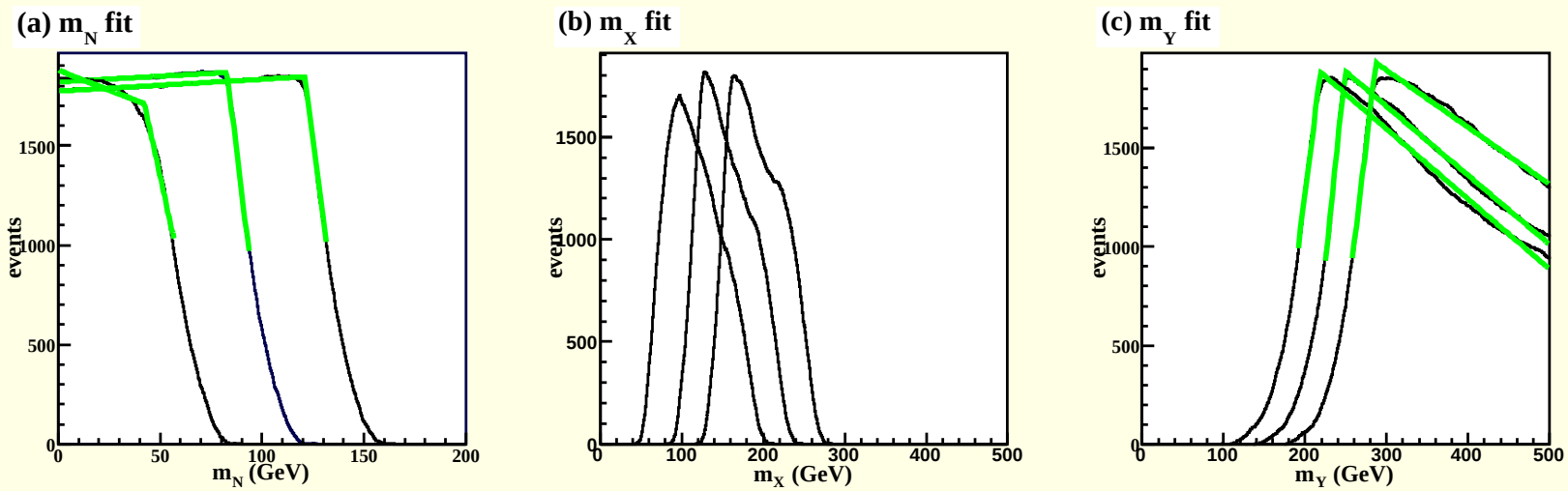

Figure 18: *A few steps showing the migration of the one dimensional fits. The middle curve in each plot corresponds to masses close to the correct values.*

3. **Each time after a fit to m_N, record the (fitted) number of events at the turning points, which is the vertical coordinate of the turning points in Fig. 17a.**
4. **Repeat step 2 and 3. The number of events recorded in step 2 will in general increase at the beginning and then decrease after some steps, as seen in Fig. 19. Stop when it has sufficiently passed the maximum position.**
5. **Fit Fig. 19 to a (quartic) polynomial and take the position where the polynomial is maximized as the estimated m_N.**
6. **Keep m_N fixed at the value in step 5 and do a few one-dimensional fits**

for m_Y and m_X until they are stabilized. Take the final values as the estimates for m_Y and m_X.

- For example, at a certain point near the correct solution, as we vary M_N, we get the following plot.

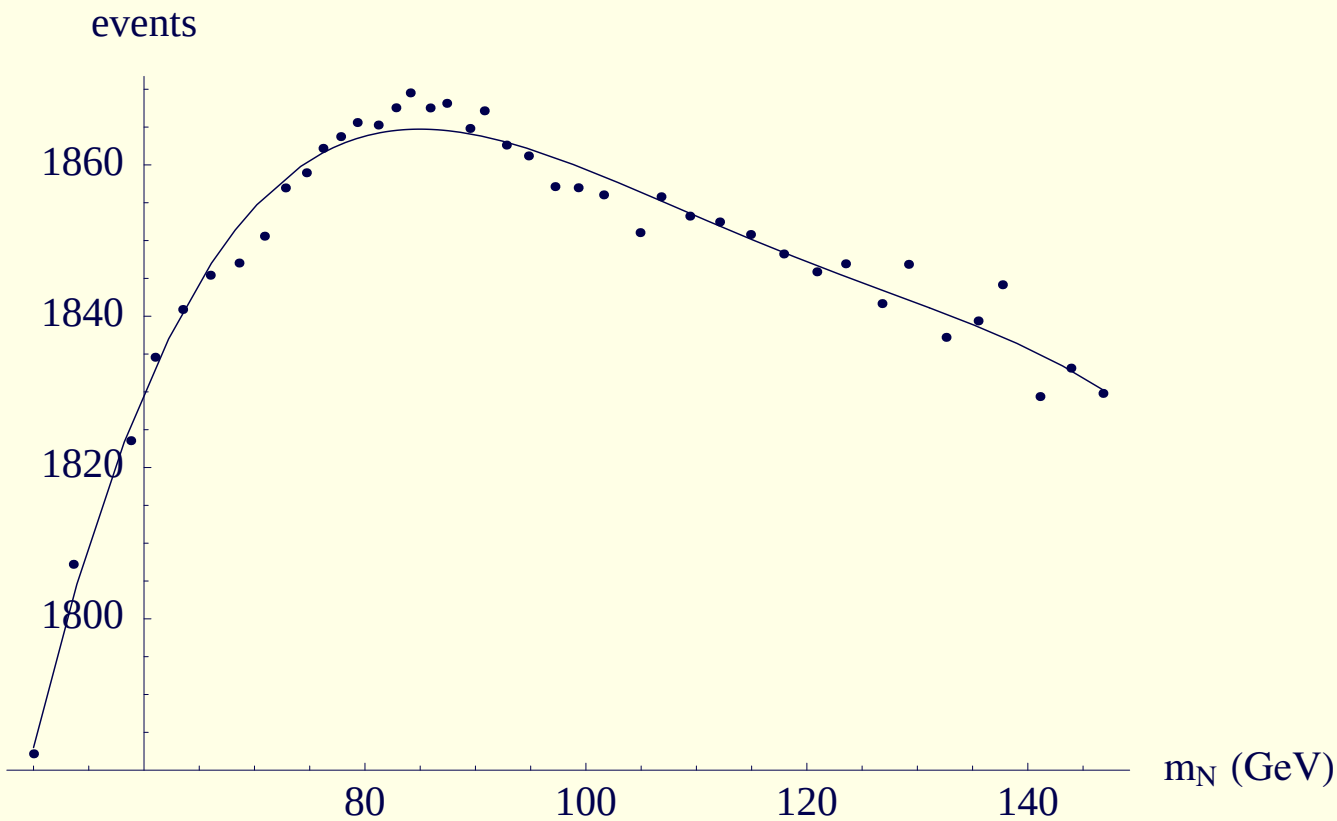

Figure 19: *Number of events consistent with M_N choice as a function of M_N.*

Remarkably, the point at which the turnover occurs gives M_N (*and* M_X and M_Y) to good accuracy.

The final values for the masses are determined as

$$\{252.2, 130.4, 85.0\}\ \mathrm{GeV} \quad vs. \quad \{246.6, 128.4, 85.3\}\ \mathrm{GeV} \tag{13}$$

Remarkably, the N mass is extremely accurate and the Y mass quite close as well.

- **Error evaluation:**

Must adopt an 'experimental' approach for such an empirical procedure:

Generate 10 different $50\ \mathrm{fb}^{-1}$ data samples and apply the procedure to each sample.

Estimate the errors of our method by examining the statistical variations of the 10 samples, which yields

$$m_Y = 252.2 \pm 4.3\mathrm{GeV}, \quad m_X = 130.4 \pm 4.3\mathrm{GeV}, \quad m_N = 86.2 \pm 4.3\mathrm{GeV}. \tag{14}$$

The statistical variations for the mass differences are much smaller:

$$\Delta m_{YX} = 119.8 \pm 1.0\text{GeV}, \quad \Delta m_{XN} = 46.4 \pm 0.7\text{GeV}. \tag{15}$$

Compared with the correct values $\mathcal{M}_A = \{246.6, 128.4, 85.3\}$, we observe small biases in the mass determination, especially for the mass differences, which means that our method has some "systematic errors".

However, these systematic errors are determined once we fix the experimental resolutions, the kinematic cuts and the fit procedure.

Therefore, they can be easily corrected for, which leaves us errors for the absolute mass scale of $\sim few$ GeV and for the mass differences of ~ 1 GeV.

- **Backgrounds**

In the above example, the background is negligible with the applied cuts.

However, if in some other case the backgrounds turned out to be substantial, they could decrease the accuracy of the mass determination.

Instead of analyzing another process with sizable backgrounds, we stick to the four muon events studied above but make up more "backgrounds".

In particular, we consider the 4-muon events from top pair production, but unlike above we do not require the muons to be isolated (which eliminates this background).

$\Rightarrow$ a significant number of events have 4 hard muons.

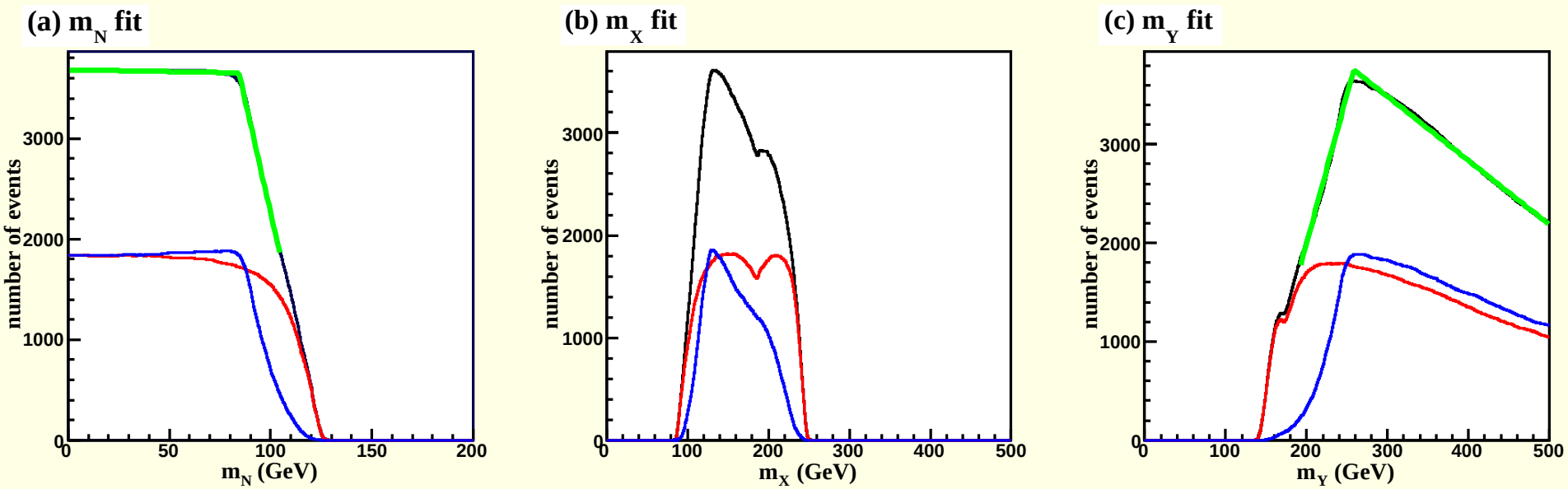

Figure 20: *Fits with $50fb^{-1}$ signal events and an equal number of background events. Separate numbers of signal (blue) and background (red) events are also shown.*

Adding an equal number of background events to $50 fb^{-1}$ signal events, we repeat the one-dimensional fits. A typical cycle around the correct masses is shown in Fig. 20.

For comparison the number of solvable signal events and background events are also shown separately.

The effect of background events is clear: the curve for solvable background events is much smoother around the turning point, and therefore smears but does not destroy the turning point.

Although we are considering one specific background process, this effect should be generic, unless the backgrounds happen to have non-trivial features around the turning points.

Nevertheless, due to the fact that there are 8 possible combinations, the chance that a background event gets solutions is quite large and they do affect the errors and biases of the mass determination.

This can be seen in Fig. 21, in which we have used the same 10 sets of signal events as in the previous subsection, but varied the number of background events according to the ratio $background/signal = 0, 0.1, 0.2, 0.5, 1$.

We observe increases in both the biases and variations.

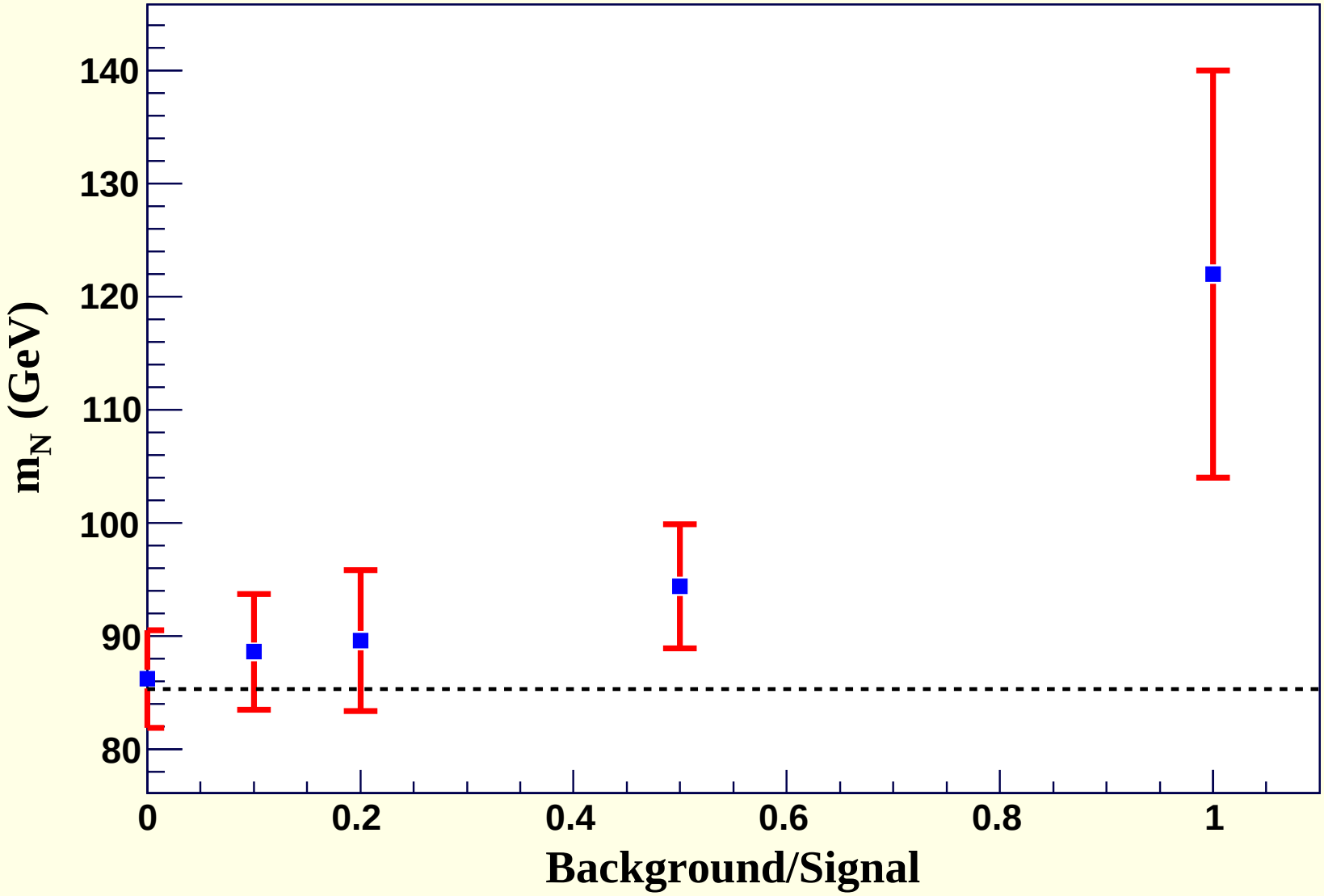

Figure 21: m_N **determination with different background-signal ratio. The dashed horizontal line corresponds to the correct** m_N**.**

- **If it should be that $m_N \sim 0$, then we must be careful.**

  We have found that it would quickly become apparent that we were not finding a maximum in the included event number as m_N is increased.

  We would then backtrack to $m_N = 0$ and find that actually the number of included events is largest there and declines as m_N increases.

- **Peculiar mass separation choices can give some special features.**

  We are currently working on optimizing our procedures for such cases.

- **We are confident that the experimental groups will actually end up doing even better in the end.**

  In particular, if they understand the backgrounds then they can separately apply our procedure to them and subtract the background from the summed curves of Fig. 20, returning us to a situation close to the zero-background case first considered.

Conclusions

- **Overall, we believe $\sim$ GeV accuracy for the absolute mass scale is achievable at the LHC.**

  1. **This should be sufficient to eliminate the 'slider' degeneracies of the LHC inverse solutions.**
  2. **Such accuracy for the more massive states will aid enormously in the GUT extrapolation.**
  3. **It will greatly increase the accuracy of the dark matter calculation.**

- **The ability to get an absolute mass scale out of LHC data could be quite crucial for determining whether the ILC500 is sufficient or one needs to go to ILC1000.**

- **Our technique can, of course, be combined with the other techniques outlined at the beginning to obtain the best possible overall mass scale and mass differences.**

- **Don't forget that we must understand how to single out a single topology (*i.e.* suppress others adequately) in the case that there are many new physics topologies.**